ELSEVIER

Polymer 43 (2002) 2409–2415

polymer

www.elsevier.com/locate/polymer

Partitioning of polymer chains in solution with a square channel: lattice Monte Carlo simulations

Peter Cifra[a], Iwao Teraoka[b,*]

[a]Polymer Institute, Slovak Academy of Sciences, Dúbravská cesta 9, 842 36 Bratislava, Slovak Republic
[b]Herman F. Mark Polymer Research Institute, Polytechnic University, Six Metro Tech Center, 333 Jay Street, Brooklyn, NY 11201, USA

Abstract

Cubic lattice Monte Carlo simulation studies were conducted to examine the effect of confinement on dilute and non-dilute solutions of polymer chains in a channel with a square cross section. In dilute solutions, the partition coefficient K_c with channels of different widths d followed the scaling-law prediction, and was close to the square of the partition coefficient K_s with a slit of the same d. The chain with its bulk radius of gyration greater than $\sim d/2$ adopted a conformation extending along the channel and, with a decreasing channel width, the chain ends were forced to face outside. The chain conformation in broader channels was a compressed random coil. The K_c increased with an increasing polymer concentration ϕ_E in the exterior solution equilibrated with the channel. In a weak confinement, K_c closely followed K_s^2 of the same ϕ_E and d. The chains contracted at higher concentrations as they did in the bulk solutions. In a strong confinement, K_c was smaller than K_s^2 at the same ϕ_E in the semidilute regime, and, at higher concentrations, sharply increased to the value close to K_s^2.

Keywords: Confinement; Partitioning; Semidilute solution

1. Introduction

Polymer chains, when confined to a small space, exhibit properties distinctly different from those in the unconfined space [1,2]. Understanding thermodynamics of confined polymer solutions is important in separation techniques at high concentrations such as high osmotic pressure chromatography [3] and phase fluctuation chromatography [4]. Because of limited accessibility to a model porous medium in experiments, thermodynamics of the confined polymer solutions have been studied primarily by using computer simulations [5–11]. In Monte Carlo simulations on a cubic lattice, we studied the partitioning of monodisperse polymer chains with a slit between two parallel impenetrable walls and static properties of the chains in the slit over a wide range of concentrations [12–18]. The focus was on the partition coefficient defined as the ratio of the polymer concentration in the slit to the one in the surrounding solution, the density profile in the slit, and the anisotropic chain dimension. Employing direct equilibration between the slit space and the free space was effective in evaluating the partition coefficient [12,15–17].

Below we summarize the thermodynamics of athermal chains in dilute and non-dilute solutions confined to a slit: (1) At low concentrations, the partition coefficient K_0 for the polymer chains of a radius of gyration R_{g0} with the slit of width d is given by $-\ln K_0 \sim (R_{g0}/d)^b$ [12,13,17] with b close to the value $1/\nu = 1.695$ predicted in the scaling theory [19]. (2) The partitioning of semidilute solution is determined approximately by the ratio of the blob size ξ (correlation length of monomer density fluctuations) to the slit width just as polymer chains in dilute solutions are partitioned according to R_{g0}/d [12,15]. As a result, the partitioning exhibits a diffuse transition from a weak penetration to a strong penetration as the decreasing ξ becomes smaller than d [20]. (3) The chain dimension in the direction parallel to the slit walls decreases with an increasing concentration. The contraction exhibits a cross-over from that of a two-dimensional chain to that of a three-dimensional chain as ξ becomes smaller than d [13,14]. (4) The monomer density decays to zero at the sites on the wall, forming a depletion layer. The layer becomes thinner with an increasing concentration [12,15,18]. (5) To bring the monomer density profile near the wall in agreement with the scaling theory prediction, a positive constant needs to be added to the distance to the wall [9–11,18]. In effect, the polymer chain sees a theoretical wall behind the physical wall on the lattice points. The constant, called the penetration depth, is 0.13–0.20 of the lattice unit at low concentrations and increases to ~0.36 in the semidilute solutions [18].

* Corresponding author. Tel.: +1-718-260-3466.
E-mail address: teraoka@poly.edu (I. Teraoka).

0032-3861/02/$ - see front matter
PII: S0032-3861(02)00040-X

The past studies of the confinement effect on the polymer chains used a slit geometry nearly exclusively [9–18]. There are only several examples that used a non-slit geometry [21–26]. Kremer and Binder [21] studied anisotropic dimensions, structure factors, and diffusion of athermal chains on a tetrahedral lattice in a square channel. Van Giessen and Szleifer [23] used cubic lattice Monte Carlo simulations to examine the anisotropic dimensions and the chemical potential of athermal chains confined to a slit and a channel. Off-lattice simulation studies were conducted in a cylindrical pore [26]. A different system of a polymer chain grafted onto an end plate of the square channel was also studied [25]. These studies examined only single-chain properties, however. Furthermore, confinement by a channel of a square cross section has not been directly compared with a hypothetical confinement that would result from two independent perpendicular slits.

In this report, we confine the polymer chains to a square channel while still employing a cubic lattice. The geometry difference is expected to make the confinement thermodynamics different from the one in the slit, especially at high concentrations. We choose a square cross section for the channel to facilitate comparison with the results obtained for the slits.

Our interest in the confinement by the channel is multifaceted: (1) For the same wall-to-wall distance, the channel provides the trapped chain with a stronger confinement effect. Channel geometry offers a good opportunity to study the effect of a strong confinement without being forced to rely on a short wall-to-wall distance. Compared at the same wall-to-wall distance, the confinement is much stronger in the channel than it is in the slit. The short wall-to-wall distance would impose a severe restriction on the conformation and arrangement of the lattice chains, especially at high concentrations, and might expose shortcomings of the lattice simulations. (2) The confining geometry is one-dimensional. Because the statistics of self-avoiding walks depends on the dimensionality of the space, the confinement by the channel will alter the solution thermodynamics in a way different from the one we have seen in the confinement by the slit. (3) Typical existing porous media have pore structures that resemble a cylindrical pore at least over a short distance, although the overall structure may be tortuous with many junctions of cylindrical sections [1].

2. Simulation methods

Cubic lattice Monte Carlo simulations were conducted for chains of $N = 100$ and 500 in a broad range of concentrations. Athermal chains were generated by using self-avoiding walks. No interaction was present between different monomers or between a monomer and a channel wall except that overlap was not allowed. The radius of gyration R_{g0} in the dilute solution limit in unconfined space is 6.524 and 16.78 for the shorter and longer chains, respectively. The unit length is a lattice spacing. The bulk overlap monomer density ϕ^*, defined as $(\phi^*/N)[2^{1/2}(R_{g0} + 0.199)]^3 = 1$, is 0.1164 and 0.0361, respectively. Addition of 0.199 to R_{g0} accounts for the correction of 'volume' occupied by each chain [13].

The simulation procedure is similar to the one employed in our preceding works [12–18]. A simple box of a channel space only was used to evaluate the density profile and the chain dimensions. A twin box consisting of a channel space with a square cross section and an unconfined space adjoining to the channel was used to obtain the partition coefficient under direct and full equilibrium condition between the free and confined spaces. The simple box has a dimension of $L_x \times L_y \times L_z (L_x = L_y;\ L_z = 150)$ with walls at $x = 0$ and $x = 1 + L_x$, and at $y = 0$ and $y = 1 + L_y$. A periodic boundary condition was enforced in the z direction. All sites in the box are available for occupancy by the monomers. The channel width d is the distance between the walls and given as $d = 1 + L_x$ and ranges between 7 and 50. Polymer chains were moved by reptation moves following the Metropolis rule [27]. In the twin box, the channel space and the unconfined space had a dimension of $L_x \times L_y \times 50$ and $50 \times 50 \times 50$, respectively ($L_x = L_y$). A periodic boundary condition was applied in all directions except where there is a channel wall. The data of the monomer density and other quantities were accumulated only after the system reached an equilibrium. Trial moves (reptation) as many as 7×10^9 were needed to obtain a smooth density profile.

3. Results and discussion

3.1. Dilute solutions

We first look at the partition coefficient K_0 in the dilute solution limit. Fig. 1 shows the confinement entropy,

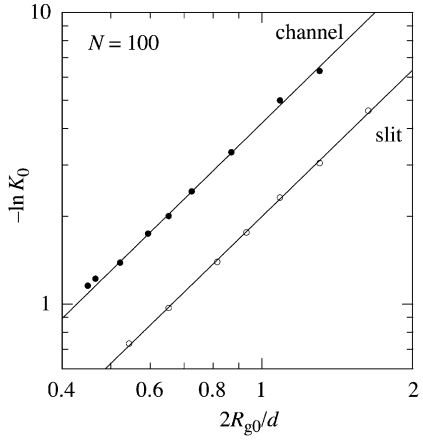

Fig. 1. Confinement entropy $-\ln K_0$ of a polymer chain of $N = 100$ in the low concentration limit, plotted as a function of the confinement strength $2R_{g0}/d$. The closed circles are for a square channel of cross section $d \times d$, and the open circles are for a slit of width d. The lines are the optimal fit by a power law.

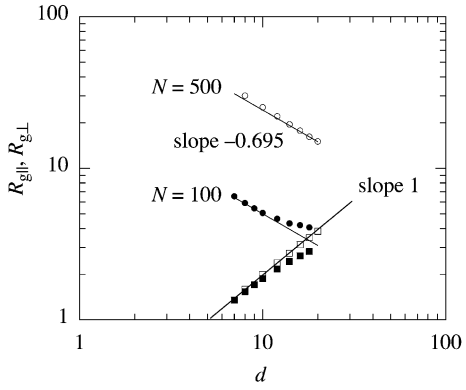

Fig. 2. The anisotropic dimensions of the confined chains of $N = 100$ (closed symbols) and 500 (open symbols), plotted as a function of the channel width d. The circles and squares denote $R_{g\|}$ and $R_{g\perp}$, the square root of the components in the mean square radius of gyration along the channel axis and parallel to one of the channels walls, respectively.

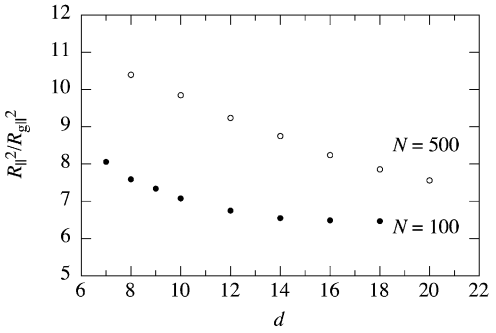

Fig. 3. The ratio of the mean square end-to-end distance and the mean square radius of gyration, both along the channel, is plotted as a function of the channel width d for chains of $N = 100$ (closed circles) and 500 (open circles).

$-\ln K_0$, as a function of the confinement strength, $2R_{g0}/d$. The closed circles were obtained in the present study for chains of $N = 100$ in equilibrium with channels of various channel widths d. The symbols are on a straight line with a slope of 1.68 ($-\ln K_0 = 4.17 \times (2R_{g0}/d)^{1.68}$), in agreement with the value predicted in the scaling theory, $1/\nu = 1.695$, and with another simulation result [23]. In the figure is also plotted the confinement entropy of the athermal chain in the slit of width d we obtained earlier [17]. The latter, shown in open circles, lie below those for the channel, indicating an easier entrance of the chain into the slit compared with the channel of the same wall-to-wall distance. The two sets of the plots are almost parallel to each other in the range plotted.

For a Gaussian chain or any other ideal chain, confinement is independent in each confinement direction. Therefore, the partition coefficient K_{c0} with a square channel of $d \times d$ is equal to the square of the partition coefficient K_{s0} with a slit of width d. In Fig. 1, the slit data almost overlap with the channel data when the former are moved up by 2.1, slightly greater than 2. The confinement of the real chain by the channel can be regarded as nearly independent in the two directions. We will discuss the small non-ideality when we compare the monomer density profile in the channel with the one in the slit.

Fig. 2 examines one-dimensional nature of the confined space. The closed and open circles in the figure show $R_{g\|}$, the square root of the z component in the mean square radius of gyration for chains of $N = 100$ and 500, respectively, as a function of d. The scaling theory [19] predicts $R_{g\|} \sim d^{1-1/\nu} = d^{-0.695}$ when $R_{g0}/d \gg 1$, which was confirmed in the past simulation studies [21,23,26]. Straight lines with a slope of -0.695 are drawn adjacent to the plots. Also shown in the figure is $R_{g\perp}$, the square root of the x component in the mean square radius of gyration. A straight line with a slope equal to one is drawn adjacent to the plots. The longer chains follow the expected $R_{g\perp} \sim d$ and closely follow $R_{g\|} \sim d^{-0.695}$. A slight upward deviation of $R_{g\|}$ is observed at small d. The shorter chains do not follow these relationships except at small d. The deviation occurs when d is larger and therefore the conformation is not sufficiently anisotropic ($R_{g\|}$ and $R_{g\perp}$ are not much different). When d is small, $R_{g\perp}$ is almost the same for the shorter and longer chains, and $R_{g\|}$ of the two chain lengths is different by a factor of the ratio of the chain lengths. It indicates that the chain conformation is approximated by a packed one-dimensional array of spheres of diameter d [19,20].

The one-dimensional chain conformation is also seen in the plot of $R_{\|}^2/R_{g\|}^2$ (Fig. 3), where $R_{\|}^2$ is the mean square of the z component of the end-to-end distance. In bulk solutions of athermal chains, the ratio (isotropic) is six at high concentrations. In dilute solutions, the ratio approaches 6.35 [28]. The confined ideal chains will have the ratio of six. If the confined chain takes a conformation uniformly extending along the channel with the two chain ends facing outside, then the ratio will be 12. The figure shows how the stronger confinement increases the ratio towards 12. The chains become increasingly extended to adopt a conformation of a one-dimensional packed array of spheres on decreasing d, especially for the longer chain. For the shorter chain, the conformation is more or less a compressed random coil, and the ratio is around 6.5 at $d = 18$. Because of the increase in the ratio in the stronger confinement, the plot of $R_{\|}$ in place of $R_{g\|}$ in Fig. 2 would give a much steeper slope as large as -1. The slight upward deviation of $R_{g\|}$ for $N = 500$ in narrow channels in Fig. 2 is also ascribed to the change in the conformation in the narrow channels. We will discuss the chain dimensions of longer chains in the channel in more details in future.

The two-dimensional monomer density profile (volume fraction of occupied sites) of chains with $N = 100$ in the channel, $\phi_c(x, y)$, is shown in Fig. 4 for different confinement strengths. Part a is in a narrow channel ($d = 20$) and part b in a wide channel ($d = 50$). The average volume fraction in the channel is 5.51×10^{-3} and 8.33×10^{-4}, respectively. The density profile has a plateau at the center

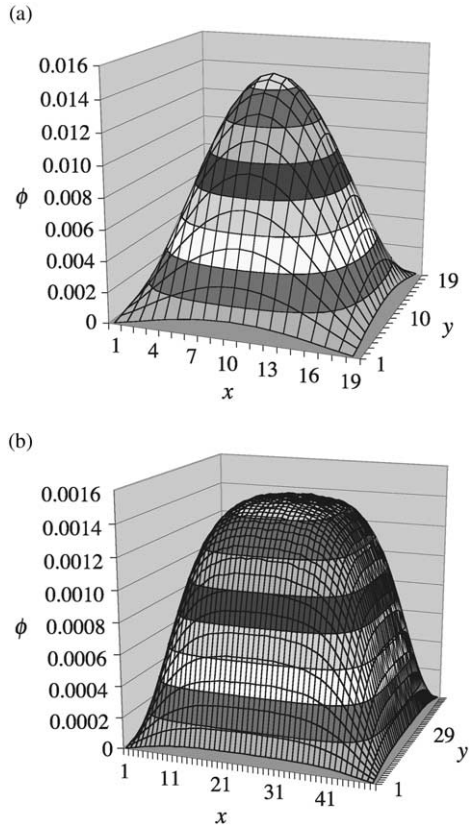

Fig. 4. Density profile $\phi_c(x, y)$ of chains of $N = 100$ in dilute solutions in (a) a narrow square channel ($d = 20$) and (b) a wide square channel ($d = 50$).

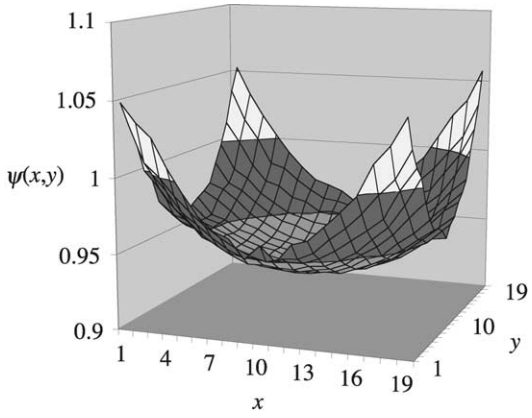

Fig. 5. Profile of $\psi(x, y)$ for the wall-to-wall distance $d = 20$. See text for the definition of $\psi(x, y)$.

in a weak confinement ($d \gg R_{g0}$), but does not when the confinement is strong.

To compare $\phi_c(x, y)$ with the density profile in the slit, we prepare a plot of

$$\psi(x, y) \equiv \frac{[\phi_c(x, y)/\phi_{cE}]}{[\phi_s(x)/\phi_{sE}][\phi_s(y)/\phi_{sE}]}$$

where ϕ_{cE} and ϕ_{sE} are the volume fractions of the chains in the surrounding solution equilibrated with the channel and the slit, respectively, and $\phi_s(x)$ and $\phi_s(y)$ are the profiles in the slits that confine the x and y directions, respectively. In this equation, $\phi_c(x, y)/\phi_{cE}$, for instance, is the probability for a site at (x,y) in the channel to be occupied, relative to the one in the exterior solution in equilibrium, by a polymer chain with a given chemical potential. For ideal chains, $\phi_c(x, y)/\phi_{cE}$ should be equal to the product of two profiles, $\phi_s(x)/\phi_{sE}$ and $\phi_s(y)/\phi_{sE}$, and therefore $\psi(x, y) = 1$ for all x and y. To see whether it is the case for athermal chains at low concentrations, we plot $\psi(x, y)$ in Fig. 5 for $d = 20$. The profile shown in Fig. 4a was used for $\phi_c(x, y)$. For $\phi_s(x)$, a low concentration profile at $\phi_I = 0.00105$ in the slit with the same d was used. Note that this $\phi_c(x, y)$ does not have a plateau in the center. Because $\phi_c(x, y)$ and $\phi_s(x)$ were obtained for the channel and slit spaces only, we evaluated ϕ_{cE} and ϕ_{sE} from the averages of $\phi_c(x, y)$ and $\phi_s(x)$ and the partition coefficients (Fig. 1). In Fig. 5, $\psi(x, y)$ is at around 0.93 at the center and edges up to around 1.05 toward the four corners. The average of $\psi(x, y)$ with respect to x and y is less than unity, in agreement with the fact that K_{c0} lies below K_{s0}^2 in Fig. 1. In a stronger confinement ($d = 12$), $\psi(x, y)$ was also concave with $\psi(x, y) = 0.66$ at the basin and 0.74 in the corners (not shown). A sharp increase in $\psi(x, y)$ in the corners was absent.

The average of $\psi(x, y)$ being less than unity and the concave profile of $\psi(x, y)$ indicate that the slit concentrates the monomers of the excluded-volume chains toward the center plane more effectively compared with the channel. The concentration at the center is easier in the slit geometry; bonded monomers can spread to the neighboring sites on the infinitely extending mid-plane. In the channel, in contrast, the spreading is not as easy, since the density must fall off to zero at the sites on the wall. It appears that the wall-to-wall distance makes a difference in the profile of $\psi(x, y)$ in the corners. Further studies are needed, since $\phi_c(x, y)$ in the corners carries a relatively large error.

Now we look at the profile $\phi_{diag}(x) = \phi_c(x, x)$ along the diagonal of the square cross section ($x = y$) and the profile $\phi_{mid}(x) = \phi_c(x, d/2) = \phi_c(d/2, y)$ along the midline between the opposite pair of walls ($x = d/2$ or $y = d/2$). The two profiles for chains of $N = 100$ are shown in Fig. 6 as a function of x in $x \le d/2$ for $d = 20$. Each profile is the average of four profiles on either side of the center of the cross section. Also shown in the profile $\phi_{slit}(x)$ in the slit of the same d at distance x from the wall.

We pay attention to the power relationship between ϕ_{diag} or ϕ_{mid} and x near the wall. Our expectation is that $\phi_{mid} \sim x^{1/\nu}$, just as $\phi_{slit} \sim x^{1/\nu}$, and therefore $\phi_{diag} \sim x^{2/\nu}$ with $\nu = 0.59$. We first notice that ϕ_{mid} is parallel to ϕ_{slit}, as expected. As in the slit [18], the slope near the wall is close to, but smaller than, the scaling prediction, $1/\nu = 1.695$. Again we see an example of the need for a positive penetration depth. Both the data for $\phi_{mid}(x)$ and $\phi_{slit}(x)$ near the wall are on a slope of 1.695 when $\gamma \simeq 0.17$ is added to x (not shown). Likewise, $\phi_{diag}(x)$ should have an asymptotic slope of $2/\nu = 3.39$. It is, however, not easy to find whether $\gamma > 0$ is

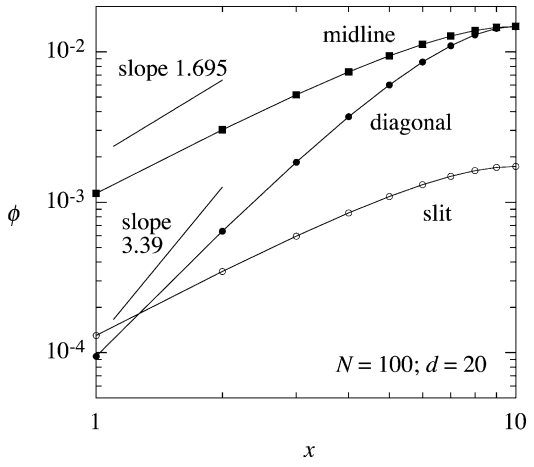

Fig. 6. Monomer density profile $\phi_{diag}(x)$ of chains with $N = 100$ along the diagonal of the square cross section of 20×20 (closed circles) and the density profile $\phi_{mid}(x)$ along the midline between the opposite pair of walls (closed squares), plotted as a function of the distance x from the wall. The lines have a slope of 1.695 and 3.39. Also shown is the density profile in a slit of the same width (open circles).

required or not for ϕ_{diag}, because the data near the corners carry a much greater error in the logarithmic scale compared with the data near the walls for ϕ_{mid}. The behavior of ϕ_{mid} and ϕ_{diag} is almost the same in the channel of $d = 50$ (not shown).

3.2. Semidilute solutions

Now we examine the effect of the polymer concentration. First, the overall partition coefficient K increases with an increasing average monomer density ϕ_E in the solution exterior to the channel. The increase is, however, slightly different from the one we observed in the partitioning with the slit. Fig. 7 compares the concentration dependence of K for chains of $N = 100$ in the channel and the slit of $d = 8$, 12, and 20. The weak-to-strong penetration transition occurs also in the channel, but the transition requires a higher ϕ_E than it does in the slit.

Fig. 8 compares the partition coefficient K for chains of $N = 100$ and 500 with the same channel of $d = 8$. The increase in K for $N = 500$ occurs at a higher concentration, but it does in a narrower range of ϕ_E, quickly approaching the K for $N = 100$. It appears that the partitioning of the semidilute solutions is governed primarily by the correlation length in the exterior solution, not by the chain length; the correlation length is determined by ϕ_E only. The sharp increase in K for $N = 500$ is noteworthy. We can expect that it will become even sharper with a further increase in N but occur at $\phi_E = \phi_t$, the threshold monomer density independent of N and to be determined later.

The scaling theory can demonstrate the independence and the sharp increase in K as follows. When the chains are sufficiently long ($R_{g0} \gg d$), the confinement entropy (divided by the Boltzmann constant) is given by $Nd^{-1/\nu}$.

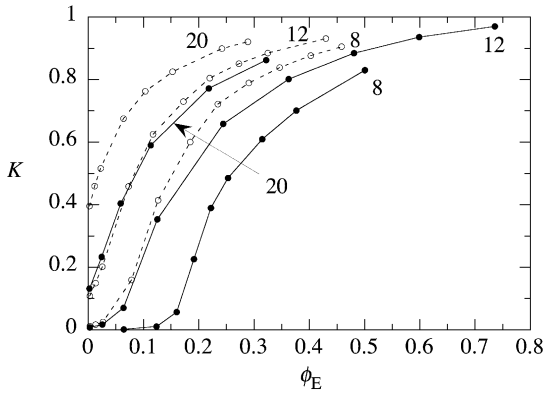

Fig. 7. Partition coefficient K of athermal chains of $N = 100$ with square channels (closed circles; solid lines), plotted as a function of the average monomer density ϕ_E in the exterior solution. The dimension d of the cross section $d \times d$ is indicated adjacent to each plot. Also shown are the partition coefficients of athermal chains of the same length with slits of width d (open circles; dashed lines).

The penetration of the chains into the channel will occur when the chemical potential in the surrounding solution increases to match the confinement entropy times temperature. The chemical potential (reduced by thermal energy) of the semidilute solution ($\phi \gg \phi^*$) is given as $(\phi/\phi^*)^{1/(3\nu-1)} \simeq N\phi^{1/(3\nu-1)}$. Thus a sharp increase in K will occur at $\phi_E = \phi_t \simeq d^{-(3-1/\nu)}$, regardless of the chain length. Note that ϕ_t shifts to a higher concentration with a decreasing d. This weak-to-strong penetration transition is not affected by the interactions between polymer chains in the channel, because the concentration in the channel is near zero. What matters are the confinement entropy and the interactions in the exterior solution only.

The next question is whether $K_c = K_s^2$ holds, compared at the same ϕ_E. If the independence of the confinement between x and y directions is valid also at finite ϕ_E, then $K_c = K_s^2$. Fig. 8 also compares K_c and K_s^2 of chains of $N = 100$

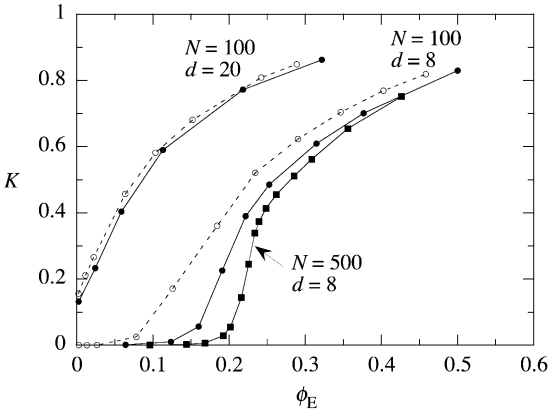

Fig. 8. The partition coefficient K_c of athermal chains of $N = 100$ with a square channel of $d \times d$ (closed circles; solid lines) at the exterior monomer density ϕ_E is compared with the square of the partition coefficient K_s of the same chains with a slit of width d (open circles; dashed lines) at the same ϕ_E. The value of d is indicated in the figure. Also shown is the partition coefficient of athermal chains of $N = 500$ (closed squares; solid line).

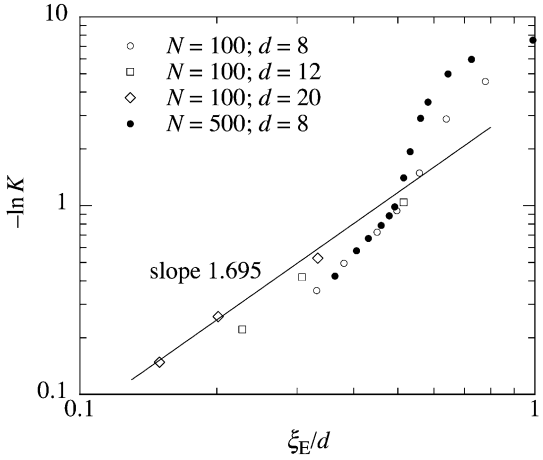

Fig. 9. The $-\ln K$, plotted as a function of ξ_E/d for the partition coefficients obtained for different chain lengths and channel widths. The line has a slope of 1.695.

for $d = 8$ and 20. In the wider channel that gives a weaker confinement, two sets of the plot run close to each other in the entire range of concentrations. In the narrower channel, however, there is a difference between the two sets. The difference maximizes at around $\phi_E = 0.15$. The smaller difference at higher concentrations indicates nearly independent partitioning of blobs in the two directions. Until the solution reaches that concentration, the independence is lost. The presence of chain–chain interactions specific to each confining geometry causes the difference. Apparently, the excess chemical potential due to the presence of other chains is higher in the channel than it is in the slit compared at the same interior concentration when the confinement is strong.

Another question is whether the partitioning is governed by the blob size relative to the channel width in the semidilute solutions. We estimate the correlation length of the exterior solution as $\xi_E = R_{g0}(\phi_E/\phi^*)^{-0.766}$. Fig. 9 shows K as a function of ξ_E/d. The data in $0.1 < \phi_E < 0.4$ are used for $N = 100$ and the data for $0.03 < \phi_E < 0.4$ for $N = 500$. The data for $N = 100$; $d = 20$ are approximately on a straight line with a slope of 1.695, but the other data are systematically deviated. It is interesting to see the data for $d = 8$ but different chain lengths run close to each other. In the slit, data in the similar plot were on a slope of 1.7 [12]. The deviation of the plot in the channel is ascribed partly to the difficulty for K to approach unity before the exterior solution becomes too much crowded. Data for broader channels ($d > 20$) would be adequate for this purpose.

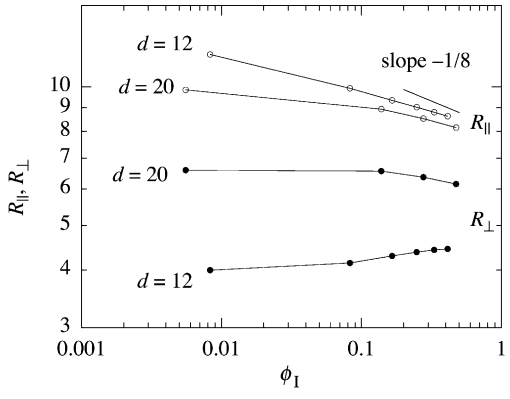

Fig. 10. The root mean square end-to-end distance of athermal chains ($N = 100$) in the channel direction, plotted as a function of the average monomer density in the slit, ϕ_I. The parallel component $R_\parallel$ (open circles) and perpendicular component $R_\perp$ (closed circles) are shown. The channel width d is indicated adjacent to each plot. The line has a slope of $-1/8$.

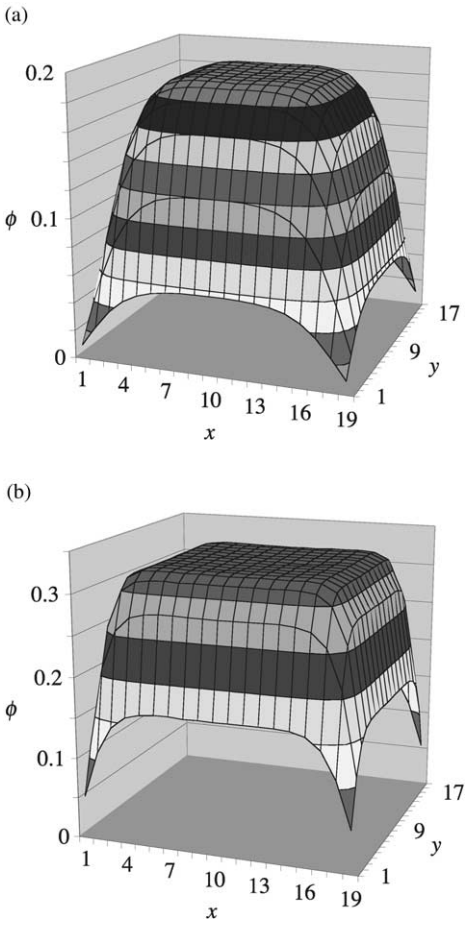

Fig. 11. Density profile $\phi_c(x, y)$ for chains of $N = 100$ in a channel of $d = 20$ at (a) $\phi_I = 0.1385$ and (b) $\phi_I = 0.2770$.

Fig. 10 shows $R_\parallel$ and $R_\perp$, the root mean square of the parallel and perpendicular components (with respect to the walls) of the end-to-end distance for chains of $N = 100$, as a function of the average monomer density ϕ_I in the channel. Two channel widths, $d = 12$ and 20, were used here. Note that these channel widths do not give a confinement sufficiently strong to extend the chain into a one-dimensional array of spheres. The conformation is a compressed coil as seen in Fig. 2. With an increasing ϕ_I, both $R_\parallel$ and $R_\perp$ decrease in the channel of $d = 20$. In the channel of $d = 12$, $R_\perp$ increases but $R_\parallel$ decreases. The increase of $R_\perp$ is due to the thinning of the depletion layer. A similar trend was

observed in the slit [13]. In $d = 20$, the anisotropy of the chain dimension is small already at low concentrations. The straight line in the figure has a slope of $-1/8$, the exponent for the contraction in unconfined chains. The contraction of the chains in the direction parallel to the channel axis approaches that of the unconfined chains at $\phi_I > 0.2$ for both $d = 12$ and 20, as the correlation length in the channel becomes shorter than d. We expect $R_\perp$ in $d = 12$ to start decreasing as well at a higher ϕ_I.

The two-dimensional density profiles in the channel are depicted in Fig. 11. The profiles are shown for chains with $N = 100$ in the channel of 20×20 at the average monomer densities of 0.1385 (a) and 0.2770 (b). The thinning of the depletion layer is evident at higher concentrations. We will discuss the density profile in the channel in more detail in another article on the mean-field Gaussian chain theory of athermal chains confined to a channel.

4. Concluding remarks

We have shown that the channel geometry allows us to see a strong confinement without being compromised by the finite lattice units in the wall-to-wall distance. We could observe a sharp increase in the partition coefficient on increasing the concentration for long chains and in a narrow channel. In the slit geometry, we have not seen such a sharp increase. The confinement by the square channel was almost independent in the two confining directions at low concentrations or at higher concentrations in the weak confinement. The monomer density profile in the channel was approximately given by the product of the density profiles in the slits in the two directions. It was not the case in the semidilute solutions in the strong confinement, but at higher concentrations, the independence was mostly regained. Mean-field Gaussian chain theory for the chains confined to a channel will be presented in a separate article to compare with the results of the simulations including those shown here. Simulation study on confinement of nonlinear chains in the slit and channel will be also interesting.

Acknowledgements

Financial support from Slovak Academy of Sciences (SAS) under 2/7076/21 and from NSF under DMR-9876360 is acknowledged. Usage of computational resources of Computer Center of SAS is acknowledged.

References

[1] Teraoka I. Prog Polym Sci 1996;21:89.
[2] de Gennes PG. Adv Polym Sci 1999;138:91.
[3] Teraoka I. Column handbook of size exclusion chromatography. San Diego: Academic Press, 1999.
[4] Lee D, Teraoka I, Fujiwara T, Kimura Y. Macromolecules 2001;34:4949.
[5] Cifra P, Bleha T, Romanov A. Makromol Chem Rapid Commun 1988;9:355.
[6] Bleha T, Cifra P, Karasz FE. Polymer 1990;31:1321.
[7] Milchev A, Paul W, Binder K. Makromol Theory Simul 1994;3:305.
[8] Thompson AP, Glandt ED. Macromolecules 1996;29:4314.
[9] Milchev A, Binder K. Eur Phys J B 1998(3):477.
[10] Milchev A, Binder K. Eur Phys J B 2000(13):607.
[11] de Joannis J, Jimenez J, Rajagopalan R, Bitsanis I. Europhys Lett 2000;51:41.
[12] Wang Y, Teraoka I. Macromolecules 1997;30:8473.
[13] Wang Y, Teraoka I. Macromolecules 2000;33:3478.
[14] Teraoka I, Wang Y. Macromolecules 2000;33:6901.
[15] Cifra P, Bleha T, Wang Y, Teraoka I. J Chem Phys 2000;113:8313.
[16] Cifra P, Bleha T. Macromol Theory Simul 2000;9:955.
[17] Cifra P, Bleha T. Macromolecules 2001;34:605.
[18] Teraoka I, Cifra P, Wang Y. Macromolecules 2001;34:7121.
[19] de Gennes PG. Scaling concepts in polymer physics. Ithaca: Cornell University Press, 1979.
[20] Daoud M, de Gennes PG. J Phys (Paris) 1977;38:85.
[21] Kremer K, Binder K. J Chem Phys 1984;81:6381.
[22] Gao J, Weiner JH. J Chem Phys 1994;100:682.
[23] van Giessen AE, Szleifer I. J Chem Phys 1995;102:9069.
[24] Hagita K, Takano H. J Phys Soc Jpn 1999;68:401.
[25] Sotta P, Lesne A, Victor JM. J Chem Phys 2000;112:1565.
[26] Sheng YJ, Wang MC. J Chem Phys 2001;114:4724.
[27] Metropolis N, Rosenbluth AW, Rosenbluth MN, Teller AH, Teller E. J Chem Phys 1953;21:1087.
[28] Olaj OF, Petrik T, Zifferer G. Macromol Theory Simul 1977;6:1277.